Am J Physiol Renal Physiol 311: F1015–F1024, 2016.
First published September 28, 2016; doi:10.1152/ajprenal.00283.2016.

Characterization and phosphoproteomic analysis of a human immortalized podocyte model of Fabry disease generated using CRISPR/Cas9 technology

Ester M. Pereira,[1]* Anatália Labilloy,[2]* Megan L. Eshbach,[2] Ankita Roy,[2] Arohan R. Subramanya,[2] Semiramis Monte,[1] Guillaume Labilloy,[3] and Ora A. Weisz[2]

[1]*Laboratory of Immunogenetics and Molecular Biology, Federal University of Piaui, Teresina, Brazil;* [2]*Renal-Electrolyte Division, Department of Medicine, University of Pittsburgh School of Medicine, Pittsburgh, Pennsylvania; and* [3]*Division of Biomedical Informatics, Cincinnati Children's Hospital Medical Center, Cincinnati, Ohio*

Submitted 5 May 2016; accepted in final form 20 September 2016

Pereira EM, Labilloy A, Eshbach ML, Roy A, Subramanya AR, Monte S, Labilloy G, Weisz OA. Characterization and phosphoproteomic analysis of a human immortalized podocyte model of Fabry disease generated using CRISPR/Cas9 technology. *Am J Physiol Renal Physiol* 311: F1015–F1024, 2016. First published September 28, 2016; doi:10.1152/ajprenal.00283.2016.—Fabry nephropathy is a major cause of morbidity and premature death in patients with Fabry disease (FD), a rare X-linked lysosomal storage disorder. Gb3, the main substrate of α-galactosidase A (α-Gal A), progressively accumulates within cells in a variety of tissues. Establishment of cell models has been useful as a tool for testing hypotheses of disease pathogenesis. We applied CRISPR/Cas9 genome editing technology to the GLA gene to develop human kidney cell models of FD in human immortalized podocytes, which are the main affected renal cell type. Our podocytes lack detectable α-Gal A activity and have increased levels of Gb3. To explore different pathways that could have distinct patterns of activation under conditions of α-gal A deficiency, we used a high-throughput antibody array to perform phosphorylation profiling of CRISPR/Cas9-edited and control podocytes. Changes in both total protein levels and in phosphorylation status per site were observed. Analysis of our candidate proteins suggests that multiple signaling pathways are impaired in FD.

CRISPR/Cas9; Fabry nephropathy; podocyte

PODOCYTES ARE KIDNEY CELLS terminally differentiated and functionally specialized in glomerular filtration. Their unique architecture shows three particularly distinct regions: *1*) the apical region, the cell body, which is found free in Bowman's space; *2*) the basal region of the cell body, which is attached to the glomerular basement membrane; and *3*) the foot processes, which grow laterally from the cell body and line the capillary loops (37). Foot processes of neighboring podocytes are firmly intertwined through a complex network of proteins called the slit diaphragm (16, 17). Upon injury, living podocytes are released from the basement membrane and the foot processes of neighboring podocytes and sloughed in the urine (33). Compensatory changes by the remaining podocytes attached to the glomerular basement membrane lead to rearrangements of their actin cytoskeleton and flattening of the foot processes (13, 33). This important structural modification is known as foot process effacement and is an early sign of podocyte injury observed in conditions associated with glomerulosclerosis and in Fabry disease (FD) (11, 38, 39, 45).

FD is an X-linked lysosomal storage disorder caused by mutations in the gene encoding the lysosomal enzyme α-galactosidase A (α-Gal A) (2, 15, 35). This enzyme catalyzes the hydrolytic cleavage of terminal α-galactosyl moieties from globotriaosylceramide (Gb3) and glycoproteins (8). The deficiency of α-Gal A leads to elevated levels of Gb3 and other glycosphingolipids in plasma and their accumulation in intracellular inclusions within many different cell types (27).

At the renal level Fabry nephropathy is classified as a metabolic podocytopathy. Kidney involvement occurs from the embryonic stage and naturally evolves to end-stage renal failure in men and in women (44). Gb3 inclusions occur in all renal cells but are distinctly more abundant in podocytes, and, in general, podocyte inclusions appear to be larger than those in other cells (6, 44). Ultrastructural morphological studies on human kidney biopsies from FD children with no nephropathy laboratory changes show podocyte foot process effacement, regarded as the cardinal feature of podocyte injury (46, 50). Podocyte effacement is a dynamic and reversible process that directly correlates with proteinuria. Early treatment of podocyte injury is essential to limit glomerular disease and progressive renal failure (1, 36). Therefore, it is highly important to develop models of human podocyte cells with the Fabry genotype and phenotype as a tool to study biological processes in a defined enviroment, without the confouding influence of hemodynamic and paracrine signals by different neighboring cell types.

With this aim, we proposed to develop a Fabry model of immortalized human podocytes using RNA-guided clustered regularly interspaced short palidromic repeats (CRISPR)-associated protein 9 (Cas9) nucleases targeting the GLA gene. With the assistance of an RFP/hygromycin-green fluorescent protein (GFP) surrogate reporter plasmid, we successfully carried out multiplex editing of two different coding regions of the GLA gene, generating podocyte line knockouts for in vitro studies. As expected, GLA knockout cells exhibited the FD biochemical phenotype, characterized by reduced α-Gal A enzyme activity and increased Gb3. Subsequently, we carried out a high-throughput screen using an array of phosphoproteins containing 1,318 antibodies against 414 phosphorylated proteins belonging to common signaling pathways. Analysis of the abundance and phosphorylation status of these proteins in gene-edited vs. control cells identifies several candidate signaling pathways that are disrupted in FD.

MATERIALS AND METHODS

Culture of kidney cell lines. Immortalized human podocytes came from Dr. Jean Daniel Sraer and were provided by Dr. Agnieszka Swiatecka-Urban (University of Pittsburgh School of Medicine, Pittsburgh, PA). These cells were isolated from a 1-mo-old normal kidney.

* E. M. Pereira and A. Labilloy contributed equally to this work.
Address for reprint requests and other correspondence: S. Monte, Campus UFPI, SG16, Ininga, 64.049-550, Brazil (e-mail: semiramis@ufpi.edu.br).

Isolation and characterization of this SV40 large-T antigen immortalized cell line is described (12). Expression of the podocyte markers podocin, WT1, Fyn, and CD2AP has been confirmed in these cells (A. Swiatecka-Urban, personal communication). Although the sex of this cell line was not reported in the original study, our data are consistent with the presence of two X chromosomes. Cells were cultured in DMEM-F-12 medium (GIBCO, Gaithersburg, MD) supplemented with 10% heat-inactivated FBS (30 min at 56°C), 2 mM L-glutamine, 1% (vol/vol) insulin-transferrin-selenium (1 mg/ml, 0.55 mg/ml, and 0.67 μg/ml, respectively; GIBCO), and 1% (vol/vol) penicillin/streptomycin (10,000 U/m; GIBCO). Podocytes were used for CRIPSR/Cas9 experiments between passages 13 and 17 from the originally immortalized cells. Cells were maintained at 37°C and 5% CO_2 in a humidified incubator and passaged at 1:10 when they reached 80% confluence.

CRISPR/Cas9 plasmid generation. Candidate single-guide RNAs (sgRNAs) targeting the first and seventh exons of *GLA* were selected using bioinformatics tools. The pHRS surrogate reporter vector was purchased from PNA Bio. The same oligonucleotide guide sequences designed for the pX330 CRISPR/Cas9 plasmid were used for the pHRS reporter plasmid, with inclusion of the PAM sequence for nuclease binding and activation. Standard desalted oligos were purchased from Integrated DNA Technologies. Each pair of complementary oligonucleotides for either pX330 or pHRS incorporation was phosphorylated and self-annealed for proper ligation (100 μM/oligonucleotide) using T4 polynucleotide kinase and T4 ligation buffer (New England BioLabs, Ipswich, MA), according to the manufacturer's protocol. Thermocycler settings were as follows: 37°C for 30 min, 95°C for 5 min, then ramping down to 25°C at 5°C/min.

The pHRS plasmid was digested with *Eco*R1-HF (New England Biolabs) and *Bam*H1-HF (New England Biolabs) in CutSmart Buffer (New England Biolabs) for 30 min at 37°C. Gel purification was performed in 1% agarose gel using Wizard SV gel and the PCR Clean-Up System (Promega) according to the manufacturer's protocol. Phosphorylated and annealed oligo duplexes (1:250 dilution) were then ligated in purified digested vector using T7 DNA ligase (New England BioLabs) at ambient temperature for 30 min according to the manufacturer's protocol.

For the pX330 plasmid, settings for cloning of phosphorylated and annealed oligos in the backbone vector were performed as a single-step digestion ligation reaction as follows: pX330, 100 ng; oligo duplex (1:250 dilution), 2 μl; Tango buffer (Thermo Scientific, Waltham, MA), 2 μl; 10 mM DTT, 1 μl; ATP, FastDigest BbsI (Thermo Scientific), 1 μl; T7 DNA ligase (New England Biolabs), 0.5 μl; and DEPC-treated H_2O added to a total volume of 20 μl. Thermocycler settings were as follows: 37°C for 5 min, 23°C for 5 min, cycling these two steps six times for a total run time of 1 h. To prevent unwanted recombination products, ligation reactions for both pHRS and pX330 vectors were treated with PlasmidSafe ATP-dependent DNase (Epicentre, Madison, WI) for 30 min at 37°C, according to the manufacturer's protocol. Ligation products (2 μl) were transformed into One Shot Stbl3 Chemically Competent *Escherichia coli* (Thermo Fischer Scientific) according to the manufacturer's protocol. Transformation products (25 or 100 μl) were seeded on ampicillin (pX330) or kanamycin (pHRS) LB agar plates. Plasmid isolation and purification was performed using a QIAprep spin Miniprep Kit (Qiagen, Valencia, CA) and QIAGEN Plasmid Maxi Kit (Qiagen), according to the manufacturer's protocol. Vector clone sequences were confirmed for oligo incorporation using Sanger Sequencing performed by the University of Pittsburgh Genomics Research Core using the hU6 and pCMV forward sequencing primers for pX330 and pHRS, respectively. Oligo incorporation into vectors was confirmed using CLC Genomics Workbench (Qiagen).

Plasmid delivery. Approximately 5×10^5 cells were seeded in six-well plates with 2 μg of pX330 plasmid and immediately transfected with 2 μg of the corresponding pHRS plasmid/well using 4 μl of lipofectamine 3000 (Invitrogen, Carlsbad, CA), 10 μl of P3000 reagent, and 1 ml of OptiMEM following the manufacturer's instructions. For concomitant delivery of pX330 and pHRS plasmids targeting the two different regions of *GLA*, 1 μg of each plasmid was used to transfect 5×10^5 cells, for a total of 4 μg of DNA. Growth medium was changed after 12 h, and experiments were performed 48–72 h after transfection.

Fluorescence-activated cell sorting. Approximately 1.5×10^6 cells cotransfected with pX330 and pHRS were trypsinized with TrypLE Select (Thermo Fischer Scientific) for 5 min, centrifuged at 500 *g* for 3 min, and resuspended in 600 μl of PBS supplemented with 10% BFS. To achieve a single-cell suspension, cells were passed through 50-μm filcon filters (BD Biosciences, San Jose, CA). Single-cell suspensions were analyzed and sorted in a BD FACSAria II (BD Biosciences), with FACSDiva version 6.1.3 software. Default setup was applied for red fluorescent protein (RFP) and GFP fluorescence detection (for GFP: 488-nm blue laser, E PMT, 502 LP mirror, 430/30 BP filter; for RFP: 488-nm blue laser, D PMT, 556 LP mirror, 585/42 BP filter). RFP/GFP double-positive cells were collected in 96-well dishes for clonal populations and/or 5×10^3 cells in 15-ml conical tubes, both containing specific growth medium.

Hygromycin treatment. For hygromycin selection, 5×10^5 human immortalized podocytes were treated 48 h after cotransfection with pHRS and pX330 plasmids with 2 mg/ml of hygromycin B (Invitrogen) in growth medium. After 48 h, the drug was removed, and the remaining viable cells were cultured in growth medium until further characterization.

Genomic DNA extraction and PCR amplification. Genomic DNA from $\sim 1 \times 10^5$ cells was extracted using QuickExtract DNA extraction solution (Epicentre) according to the manufacturer's protocol. The genomic region flanking the CRISPR/Cas9 target sites was amplified by PCR using Phusion High-Fidelity DNA Polymerase (New England BioLabs) using 5 μl of extracted genomic DNA as a template. Primer sets flanking the target regions of the GLA gene were designed using NCBI Primer Designing. A touchdown approach was used for enhanced specificity and yield (28). The sequences of the oligonucleotides used in this study are listed in Table 1. The following settings were applied: 30 s at 98°C; 15 cycles at 98°C for 10 s, 67°C for 30 s (reducing annealing temperature by 1°C each cycle), and 72°C for 30 s; followed by 25 cycles at 98°C for 10 s, 52°C for 30 s, and 72°C for 30 s; and a final cycle of 72°C for 10 min. PCR products were separated in a 2% agarose gel stained with SYBR Safe DNA Gel Stain (Thermo Fischer Scientific) and visualized on a Molecular Imager Gel Doc XR System (Bio-Rad Laboratories, Munich, Germany). Images were processed using Image Lab 5.1 Software (Bio-Rad Laboratories).

CRISPR/Cas9 clone mutation analysis. Genomic DNA extracted from clones as described above and the region flanking the CRISPR/Cas9 target sites were amplified by PCR using GoTaq Green Master Mix (Promega). The sequences of the oligonucleotides used are listed

Table 1. *Oligonucleotides and primers used in this study*

Region	Plasmid	Sequence 5′-3′
R1 (exon 1)	pX330	F: CACCGATAAATTTCCGCGGGTAACC
		R: AAACGGTTACCCGCGGAAATTTATC
	pHRS	F: AATTCTCCAGGTTACCCGCGGAAATTTATAGGAG
		R: GATCCTCCTATAAATTTCCGCGGGTAACCTGGAG
	PCR	F: ACGGCTATAGCGAGACGGTA
		R: GGGTCTGAATAGAACCGGGC
R2 (exon 7)	pX330	F: CACCGTGTGGGAACGACCTCTCTC
		R: AAACGAGAGAGGTCGTTCCCACACC
	pHRS	F: AATTCTGTGTGGGAACGACCTCTCTCAGGAGGAG
		R: GATCCTCCTCCTGAGAGAGGTCGTTCCCACACAG
	PCR	F: GACCAGGGGGTTGGAATGAC
		R: AGCTGAAGCAAAACAGTGCC

F, forward; R, reverse.

in Supplemental Table S1 (Supplemental data for this article can be found on the Journal website.). Bands were excised from the resulting agarose gel and purified using Wizard SV Gel and the PCR Clean-Up System (Promega) according to the manufacturer's protocol. The pGEM-T Easy Vector System (Promega) was used according to the manufacturer's protocol for insertion/ligation of the purified PCR products in the pGEM-T Easy vector. The ligation reaction products were transformed into MAX Efficiency DH5α Competent Cells (Invitrogen), and transformation products were seeded on ampicillin LB agar plates. Plasmids were purified from individual colonies using the QIAprep spin Miniprep Kit (Qiagen) according to the manufacturer's protocol and sequenced using the T7 forward sequencing primer. Mutation analysis was completed using CLC Genomics Workbench (Qiagen).

T7 endonuclease I assay. Target site PCR amplicons were hybridized by denaturing and reannealing to allow for homo- and heteroduplex formation. Briefly, 1.6 μg of PCR products were resuspended in a final volume of 10 μl in 1× Phusion High Fidelity PCR buffer (New England Biolabs), and duplicate samples were amplified in a thermocycler using the following settings: 95°C for 10 min, then ramp down to 85°C, and decreasing at 2.0°C/s. After that, the temperature was dropped 10°C at a time at a rate of 0.3°C/s, maintaining target temperatures for 1 min until reaching 25°C. Hybridized products were then digested with T7 endonuclease I (T7E1), which recognizes mismatch and cleaves it (New England BioLabs) at 37°C for 15 min. Products were separated on a 2% agarose gel and scanned on a Molecular Imager Gel Doc XR System (Bio-Rad Laboratories). Images were processed using Image Lab 5.1 Software (Bio-Rad Laboratories).

Indirect immunofluorescence. Podocytes (2.5×10^4 cells) were seeded on cover slips coated with 10% PureCol type I bovine collagen solution (Advanced BioMatrix, Carlsbad, CA) in growth medium in 12-well cell culture dishes. After 24 h, cover slips were fixed with 10% neutral buffered formalin solution (Sigma-Aldrich, St. Louis, MO) for 15 min, quenched for 5 min in 50 mM NH_4Cl and 0.1 M glycine in PBS, and permeabilized with 0.1% Triton X-100 (Sigma-Aldrich) in quench solution for 8 min. The samples were then blocked for 1 h in 1% BSA (Sigma-Aldrich) and 0.1% saponin (Sigma-Aldrich) in PBS. Next, the cover slips were incubated with primary antibody anti-CD77 (Ab35768 rat monoclonal IgM, Abcam dilution 1:50) for 1 h and then washed two times quickly with PBS followed by washing three times for 5 min in PBS containing 0.5% BSA (Sigma-Aldrich) and 0.05% saponin (Sigma-Aldrich) in a shaker. Cover slips were then incubated with secondary antibodies (Cy3 goat anti-rat dilution 1:250) for 30 min. All steps were performed at room temperature. The cover slips were mounted on slides with ProLong Gold Antifade Reagent with DAPI (Invitrogen). Images were captured using identical settings using a Leica DM6000 B fluorescence upright microscope system (Leica Microsystems, Buffalo Grove, IL) and processed equivalently using Volocity 6.1 Software (PerkinElmer, Waltham, MA).

Enzyme activity assay. α-Gal A activity was measured fluorimetrically in control and CRISPR/Cas9 modified (Fabry) immortalized human podocytes using 4-methylumbelliferyl-α-D-galactopyranoside (Sigma) as the substrate. This artificial substrate in a citrate phosphate buffer is hydrolyzed by the α-Gal A in cells to 4-methylumbelliferone and galactose (31). Approximately 10^6 cells were pelleted in a microcentrifuge tube at 800 *g* for 3 min, washed one time in PBS and Dulbecco's solution minus Mg^{2+} and Ca^{2+}, and repelleted. Cells were then lysed by three cycles of freeze-thaw in 500 μl of citrate-phosphate buffer (50 mM citric acid monohydrate, 100 mM dibasic sodium phosphate-anhydrous, pH 4.8), vortexing for 15 s between freeze cycles. Protein concentration was measured in a BioPhotometer (Eppendorf) using the protein direct photometric measurement setting at 280 nm. Equal amounts of protein were used to measure enzyme activity. Lysates (50 μl) were incubated with 20 μl of substrate solution [5 mM 4-methylumbelliferyl-α-D-galactopyranoside (Sigma-Aldrich) and 100 mM *N*-acetylgalactosamine (Sigma-Aldrich) in DEPC-treated water] for various times (1 h at 37°C or 6 and 24 h at room temperature). To assess linearity of the assay, four reactions were set up by mixing 0, 5, 25, or 50 μl of lysate of control cells with 50, 45, 25, or 0 μl of lysate that previously inactivated at 100°C for 10 min for enzyme inactivation. These reactions corresponded to 0, 10, 50, and 100% of enzyme activity in control cells, respectively. Enzymatic activity was terminated by addition of 70 μl of 50 mM glycine ammonium hydroxide, pH 10.5. The fluorescence intensity of released 4-methylumbelliferone was quantified in a GloMax-Multi+ Detection System with Instinct Software at 360–380 nm excitation/500 nm emission.

Phosphospecific antibody microarray. Phospho-Explorer Antibody Arrays and the Antibody Array Assay Kit were obtained from Full Moon Biosystems. Experiments were performed according to the manufacturer's protocol using the solutions provided. Approximately 5×10^6 control and GLA-edited (FD) immortalized podocyte cells (Clone PCF1) were pelleted by centrifugation at 500 *g* for 2 min at 4°C and washed three times with ice-cold PBS. Proteins were extracted by adding 200 μl of nondenaturing lysis buffer and lysis beads to the pellet, followed by five cycles of vortexing for 1 min and incubating on ice for 10 min. Lysates were centrifuged at 10,000 *g* for 5 min at 4°C, and the supernatants were transferred to fresh tubes. Lysates (100 μl) were then purified using provided previously hydrated affinity columns centrifuged at 750 *g* for 2 min. Purified lysates were frozen at −80°C for 10 min and immediately centrifuged at 16,100 *g* for 15 min at 4°C. Lysate protein concentration was measured using UV absorbance spectroscopy at 280 nm using a NanoDrop Spectrophotometer (Thermo Scientific). Lysate quality control was verified by the presence of two well-separated peaks at 200–230 and 240–280 nm. Cell lysates (80 μg of protein resuspended in 75 μl of labeling buffer) were incubated with biotin solution (10 μg/μl in *N,N*-dimethylformamide) for 2 h at room temperature, vortexing for 15 s every 10 min. Stop reagent (35 μl) was then added to biotinylated samples, which were then vortexed for 15 s, quickly spun, and incubated at room temperature for 30 min, vortexing for 15 s every 5 min. Microarray slides were blocked with blocking solution (30 ml) for 45 min on an orbital shaker at 55 revolutions/min (rpm) at room temperature and then rinsed 10 times with ddH_2O in a 50-ml conical tube, shaking for 10 s each time. Slides were then immersed in 6 ml of protein coupling solution mixed with biotinylated lysate and incubated for 2 h on an orbital shaker at 55 rpm at room temperature. Slides were then transferred to a petri dish containing 30 ml of wash solution, washed three times for 10 min on an orbital shaker at 55 rpm at room temperature, and then rinsed 10 times with ddH_2O in a 50-ml conical tube, shaking for 10 s each time. Next, slides were incubated in solution containing 30 μl of Cy3-streptavidin (0.5 mg/ml; GE Healthcare) in 30 ml of detection buffer in an aluminum foil-covered petri dish for 20 min on an orbital shaker at 35 rpm. Slides were then transferred to a petri dish containing 30 ml of wash solution and washed two times for 10 min and then one time overnight rotating on an orbital shaker at 55 rpm at room temperature, then rinsed 10 times with ddH_2O in a 50-ml conical tube, shaking for 10 s each time. Slides were dried by centrifugation, placing each slide in a 50-ml conical tube and centrifuging them at 1,300 *g* for 10 min. Slides were scanned on a GenePix 4000B Microarray Scanner (Molecular Devices) at 500 PMT, and fluorescence quantification information was extracted using GenePix Pro 6.0 Software (Molecular Devices).

Microarray data analysis. Data mining was performed using the R environment version 3.0 (49). Median fluorescence signal at wavelength 532 minus the local background at wavelength 532 (F532-B532) for each feature (i.e., area of interest in image analysis) was used for calculations. For comparison of total protein abundance and phosphorylation between control and gene-edited podocytes, fold changes of normalized median fluorescence values for each corresponding feature were calculated by dividing the value obtained for GLA-edited podocyte lysates by the value obtained for control cells

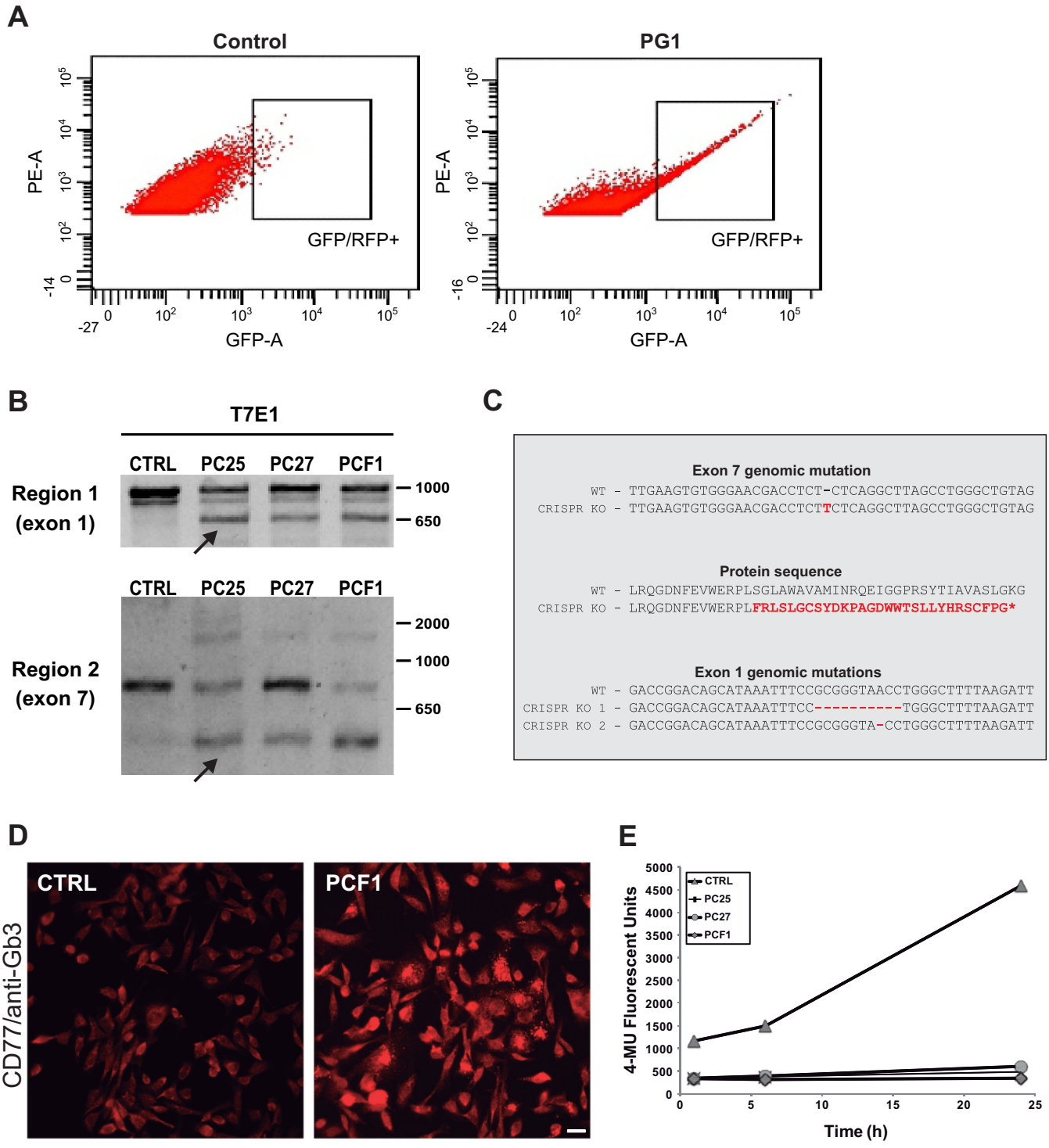

Fig. 1. Characterization of CRISPR/Cas9 GLA-edited immortalized human podocytes. *A*: immortalized human podocyte cells were transfected with either empty pX330 and pHRS plasmids (CTRL) or PX330 targeting GLA gene regions 1 and 2 along with respective pHRS plasmids. Cells underwent a first round of cotransfection with the pX330 plasmid targeting region 2 and corresponding pHRS plasmid and were sorted by flow-assisted cell sorting (FACS) for red fluorescent protein (RFP)/enhanced green fluorescent protein (eGFP) positivity. *B*: T7 endonuclease I (T7E1) assay. PCR amplicons for control and GLA podocyte populations were denatured and hybridized by heat and cooling, digested with T7E1, and separated on a 2% agarose gel. *C*: regions surrounding the guide sequences used to generate PCF1 cells were sequenced as described in MATERIALS AND METHODS. A single nucleotide insertion (highlighted in red) was consistently detected within exon 7 of the GLA genomic DNA, leading to an amino acid frameshift at amino acid 345 that alters the majority of the β-domain of α-galactosidase A (α-Gal A) and leads to early termination. Two deletions were found within the exon 1 targeted region. The effect of these mutations on expression is unknown, since they are upstream of the translation start site. The genomic sequences shown are correlated to nucleotides 101398045–101398089 (exon 7) and 101407913–101470958 (exon 1) in the human GRCH38.p7 reference sequence. *D*: immunofluorescence of CD77/Gb3 of control and GLA CRISPR/Cas9 podocyte cell population showing accumulation of Gb3 in GLA CRISPR/Cas9 podocyte cells. Scale bar = 15 μm. *E*: α-Gal A enzyme activity. Cell lysates of control and GLA CRISPR/Cas9 podocyte cell populations were incubated with 4-methylumbelliferyl-α-D-galactopyranoside and *N*-acetylgalactosamine for the various time points (1, 6, and 24 h). α-Gal A enzyme activity was quantified as fluorescence intensity units of released 4-methylumbelliferone (4-MU).

Table 2. *Phosphoproteins that showed increased total abundance in Fabry disease podocytes compared with control podocytes*

Protein (Official Full name)	Gene Symbol	Log2, fold change
Integrin, β_1 (fibronectin receptor, beta polypeptide)	ITGB1	1.02
Paxillin	PXN	0.58
Gab2 (GRB2-associated binding protein 2)	GAB2	0.50
IR (insulin receptor)	INSR	0.41
EGFR (epidermal growth factor receptor)	EGFR	0.36
eIF4E (eukaryotic translation initiation factor 4E)	EIF4E	0.34
Stathmin 1	STMN1	0.33
IkB - β (nuclear factor of κ light polypeptide gene enhancer in B cells inhibitor, β)	NFKBIB	0.27
TGFBR1 (transforming growth factor, β receptor 1)	TGFBR1	0.27

followed by a log2 transformation. Transformed fold change values greater than or equal to 0.26 (i.e., upregulated by a factor of 1.2) or lesser than or equal to −0.26 (i.e., downregulated by a factor of 1.2) were considered significant. Shapiro-Wilk test with α of 0.05 was used to test for normality.

Microarray analysis quality control. A conservative approach was used throughout the quality control process to minimize false positive results. Only true values of fluorescence were used for further analysis. Measurements were considered true values when the fluorescence signal for each spot was greater than three times the average of the median fluorescence signal of empty spots. When normalized fluorescence of replicates for a certain variable had values that overlapped between gene-edited podocytes and control podocytes, a value of 1 was attributed to the fold change (i.e., no difference between control and gene-edited podocytes). Because a noticeable proportion of variables showed coefficient of variation between replicates >0.2, the fold changes were calculated by using values that showed minimal difference between gene-edited and control podocytes. In total protein analysis, for proteins that were represented more than one time (i.e., several total antibodies against the same protein), the most conservative number was used for analysis (i.e., the fold change value that was closest to 1). When fold change showed conflicting results among different epitopes representing the same protein (i.e., fold change results showing that same protein underwent both up- and downregulation), these proteins were excluded from further analysis. Verification of expression of each individual protein in podocytes was performed using the Mouse Podocyte mRNA Database (available at http://helixweb.nih.gov/ESBL/Database/Podocyte_Transcriptome/index.htm) (25) and the NCBI Gene Expression Omnibus (GEO) Database (5, 14).

Enrichment analysis. Site-specific information on protein regulation, upstream kinases and/or phosphatases, and expected biological action was obtained using PhosphoSitePlus (Cell Signaling Technology) (20). Functional annotation, gene ontology functional classification, clustering, and pathway analysis of significant data (transformed fold change values greater than or equal to 0.26 or lesser than or equal to −0.26) were performed using Database for Annotation Visualization and Integrated Discovery (DAVID) Bioinformatics Resources 6.7 (National Institute of Allergy and Infectious Diseases, National Institutes of Health) (22), considering all proteins tested in the array as the background population.

RESULTS

Human immortalized podocytes are successfully edited with CRISPR/Cas9. CRISPR/Cas9 technology enables selective editing of genomic DNA leading to gene disruption by nonhomologous end joining. Using bioinformatics tools, we designed two sgRNAs against the first and seventh exons of the human GLA gene and cloned them into the pX330 plasmid. First, we cotransfected immortalized human podocytes with either CRISPR/Cas9 pX330 plasmids targeting the GLA exon 7 or empty pX330 plasmids and with the surrogate reporter plasmid pHRS, which enables enrichment for cells with CRISPR/Cas9-induced modifications by cotransfection. The pHRS plasmid contains cassettes for mRFP expression, the same CRISPR/Cas9 genome target nucleotide sequence (in this case, targeting the GLA exon 7), and an eGFP-hygromycin resistance fusion protein. The plasmid is designed so that mRFP is expressed constitutively, whereas the enhanced GFP (eGFP) and hygromycin genes are out-of-frame and preceded by a stop-codon and a self-cleaving 2A peptide. In the absence of plasmid editing, mRFP will be expressed, but transfected cells will lack eGFP expression and hygromycin resistance. Double-stranded breaks (47) at the target sequence of the plasmid by CRISPR/Cas9 and subsequent indel cause a frameshift, which enables eGFP expression and hygromycin resistance. This provides two straightforward approaches (FACS and drug resistance) to enrich for gene-edited cell populations, since modification of this reporter plasmid mirrors genomic modification in the cells (40). Forty-eight hours after cotransfection of plasmids, ~4% of the podocytes expressed mRFP, demonstrating moderate transfection efficiency of the reporter plasmid. A small proportion of the Mrfp-positive cells were also positive for eGFP fluorescence by FACS, indicating that frameshifting indel changes were incorporated in the reporter plasmid, inducing translation of eGFP (Fig. 1*A*). The efficiency of plasmid modification, characterized by eGFP expression, varied from 15 to 18%, corresponding to 0.8 to 1.6% of the starting population (data not shown). However, despite being genetically modified, when we carried out the dosage of enzyme activity of α-GAL A, these cells showed only a reduction of 50% of the enzyme activity (data not shown). To obtain a more complete knockout of GLA, these cells were retransfected with pX330 plasmids targeting both exons 1 and 7 along with the corresponding surrogate reporter pHRS plasmids. After selection in hygromycin, cell populations isolated using cloning cylinders were tested for genome editing using T7E1 assay (Fig. 1*B*). T7E1 endonuclease, an enzyme that recognizes and cleaves mismatched DNA, is used to digest heteroduplexes. The resulting cleaved and full-length PCR products are visualized by gel electrophoresis. As shown in Fig. 1*B*, T7E1 endonuclease assay analysis demonstrated the presence of different bands in all CRISPR/Cas9 GLA podocyte cell populations, suggesting generation of missmatches. Several of the cell populations that showed changes within both targeted regions (PC25, PC27, and PCF1) were subjected to additional characterization. Additionally, the targeted regions of GLA were sequenced in PCF1 cells to verify mutations at these sites (Fig. 1*C*).

CRISPR/Cas9-mediated GLA editing of immortalized human podocytes results in α-Gal A deficiency and accumulation of globotriaosylceramide. Loss-of-function mutations in the GLA gene associated with FD result in the inability of the α-gal A enzyme to metabolize neutral glycosphingolipids with α-D-galactosyl residues, chiefly globotriaosylceramide (Gb3/CD77). To assess the phenotype of the generated CRISPR/Cas9 GLA-edited podocyte cell lines, enzyme activity and anti-CD77 staining were performed. First, we examined Gb3 levels in a mixed population of gene-edited podocytes that were selected using FACS sorting. In FD, Gb3/CD77 is known to progressively accumulate in kidney cells, a process that can

Table 3. *Phosphoproteins that showed decreased total abundance in Fabry disease podocytes compared with control podocytes*

Protein (Official Full Name)	Gene Symbol	Log2, fold Change
p53 (tumor protein p53)	TP53	−0.51
BTK (bruton agammaglobulinemia tyrosine kinase)	BTK	−0.49
Survivin (baculoviral IAP repeat containing 5)	BIRC5	−0.37
HER2 (Erb-b2 receptor tyrosine kinase 2)	ERBB2	−0.37
NFkB-P65(V-rel avian reticuloendotheliosis viral oncogene homolog A)	RELA	−0.35
PAK4 [p21 protein (Cdc42/Rac)-activated kinase 4]	PAK4	−0.35
FKHR/FOXO1A (forkhead box O1)	FOXO1	−0.34
Smad2 (SMAD family member 2)	SMAD2	−0.33
FAK (protein tyrosine kinase 2)	PTK2	−0.33
PDGFR beta (platelet-derived growth factor receptor, β polypeptide)	PDGFRB	−0.32
MAP3K8/COT (mitogen-activated protein kinase kinase kinase 8)	MAP3K8	−0.32
ASK1 (mitogen-activated protein kinase kinase kinase 5)	MAP3K5	−0.31

begin in utero and which results in tissue damage, often culminating in kidney failure (52). Indirect immunofluorescence staining of podocytes with anti-CD77 antibody revealed strikingly elevated levels of the glycosphingolipid in CRISPR/Cas9-edited podocytes compared with control cells, confirming a substantial increase in the substrate for α-gal A in these cells (Fig. 1*D*).

Additionally, we found no detectable α-gal A enzyme activity assay in our CRISPR/Cas9 GLA-edited podocyte cell populations (Fig. 1*E*). As a positive control, we confirmed that activity of α-mannosidase in our CRISPR/Cas9 GLA cell population was preserved (data not shown) (30). Together, these findings suggest that we have a valid cell model of podocytes with the genotype and phenotype of FD.

Because glycosphingolipids play central roles in adhesion, migration, and cell signaling, we wondered whether the accumulation of Gb3 in FD podocytes causes chronic alterations in signaling pathways with consequences on cell function and viability. To answer this question, we used a phosphoarray approach to examine steady-state changes in cellular signaling pathways.

Phosphoarray analysis of CRISPR/Cas9 GLA-edited and control podocytes. An antibody microarray was performed using lysates prepared from control and CRISPR/Cas9 GLA-edited human immortalized podocytes as described in MATERIALS AND METHODS. The array contains 1,318 total and phosphorylation-specific antibodies against 414 different proteins and 686 phosphorylation sites in duplicate, allowing for high-throughput parallel analysis of abundance and phosphorylation of those proteins. We first compared the total abundance of these signaling proteins between gene-edited and control podocytes by calculating the fold change for each individual epitope using the conservative strategy described in MATERIALS AND METHODS. This analysis demonstrated that 21 phosphoproteins in the array showed differences in total protein abundance. Nine phosphoproteins showed increased total protein abundance in CRISPR/Cas9 GLA-edited podocytes (Table 2), whereas 12 proteins had decreased levels compared with control podocytes (Table 3).

With the use of a similar approach to compare changes in phosphorylation of signaling proteins between gene-edited and control podocytes, a total of 43 proteins with differences in phosphorylation at 51 specific sites were identified. Increased phosphorylation in CRISPR/Cas9 GLA-edited podocytes was noted in 13 phosphorylation sites of 12 different proteins (Table 4), and decreased phosphorylation was observed in 38 sites of 33 different signaling proteins (Table 5). Some proteins showed both an increase and decrease in phosphorylation at different sites.

Gene ontology (GO) enrichment analysis was performed using positive array findings in either abundance or phosphorylation among gene-edited and control podocytes (3). Table 6 shows the top five hits in enrichment analysis based on GO terms for CRISPR/Cas9 GLA-edited podocytes compared with control podocytes. These genes show only modest fold enrichment to the background gene population on the array. Clustering analysis of the candidate proteins at DAVID, including all 59 proteins that showed differences in either total abundance or phosphorylation and taking into account all proteins in the array, as the background gene population revealed a total of 73 enrichment clusters. None of these clusters reached an enrich-

Table 4. *Phosphorylation sites and respective phosphoproteins that showed increased fluorescence in Fabry disease podocytes compared with control podocytes*

Protein (Official Full Name)	Phosphorylation Site	Gene Symbol	Log2, fold change
P90RSK (ribosomal protein S6 kinase, 90 kDa, polypeptide 1)	Phospho-Thr^{359}/Ser^{363}	RPS6KA1	1.23
HSP27 (heat shock 27-kDa protein 1)	Phospho-Ser^{82}	HSPB1	0.84
CBL (Cbl protooncogene, E3 ubiquitin protein ligase)	Phospho-Tyr^{700}	CBL	0.88
IKK-beta (inhibitor of κ light polypeptide gene enhancer in B cells, kinase β)	Phospho-Tyr^{188}	IKBKB	0.86
Synuclein, α	Phospho-Tyr^{133}	SNCA	0.58
PKC-δ (protein kinase C, δ)	Phospho-Ser^{645}	PRKCD	0.50
p38 MAPK (mitogen-activated protein kinase 14)	Phospho-Tyr^{182}	MAPK14	0.49
CD3Z (CD247 molecule)	Phospho-Tyr^{142}	CD247	0.46
NF-kB-p65 (V-rel avian reticuloendotheliosis viral oncogene homolog A)	Phospho-Ser^{536}	RELA	0.44
SMAD family member 3	Phospho-Ser^{204}	SMAD3	0.43
PDGFR-β (platelet-derived growth factor receptor, β-polypeptide)	Phospho-Tyr^{751}	PDGFRB	0.42
STAT5A (signal transducer and activator of transcription 5A)	Phospho-Ser^{725}	STAT5A	0.42
IKK-β (inhibitor of κ-light polypeptide gene enhancer in B cells, kinase β)	Phospho-Tyr^{199}	IKBKB	0.38

Table 5. *Phosphorylation sites and respective phosphoproteins that showed decreased fluorescence in Fabry disease podocytes compared with control podocytes*

Protein (Official Full Name)	Phosphorylation Site	Gene Symbol	Log2, fold change
HER2 (Erb-b2 receptor tyrosine kinase 2)	Phospho-Tyr^{877}	ERBB2	−1.44
MEK1 (mitogen-activated protein kinase kinase 1)	Phospho-Ser^{217}	MAP2K1	−1.34
TYK2 (tyrosine kinase 2)	Phospho-Tyr^{1054}	TYK2	−0.90
Rb (retinoblastoma 1)	Phospho-Ser^{807}	RB1	−0.62
CD45 (protein tyrosine phosphatase, receptor type, C)	Phospho-Ser^{1007}	PTPRC	−0.61
Mst1/Mst2 (serine/threonine kinase 4)	Phospho-Thr^{183}	STK4/STK3	−0.60
Synaptotagmin I	Phospho-Thr^{202}	SYT1	−0.60
HDAC1 (histone deacetylase 1)	Phospho-Ser^{421}	HDAC1	−0.57
Rb (retinoblastoma 1)	Phospho-Thr^{821}	RB1	−0.57
ATP citrate lyase	Phospho-Ser^{454}	ACLY	−0.57
Tau (microtubule-associated protein-τ)	Phospho-Thr^{212}	MAPT	−0.56
JAK1 (Janus kinase 1)	Phospho-Tyr^{1022}	JAK1	−0.56
KCNIP3 (Kv channel-interacting protein 3, calsenilin)	Phospho-Ser^{63}	KCNIP3	−0.51
HDAC2 (histone deacetylase 2)	Phospho-Ser^{394}	HDAC2	−0.57
BAD (BCL2-associated agonist of cell death)	Phospho-Ser^{134}	BAD	−0.46
PKC-β (protein kinase C, β)	Phospho-Ser^{661}	PRKCB	−0.42
p44/42 MAPK (mitogen-activated protein kinase 3)	Phospho-Thr^{202}	MAPK3	−0.42
Ephrin-B1/B2/B3	Phospho-Tyr^{324}	EFNB1/2/3	−0.40
STAT3 [signal transducer and activator of transcription 3 (acute-phase response factor)]	Phospho-Ser^{727}	STAT3	−0.38
p53 (phospho-Ser^{315})	Phospho-Ser^{315}	TP53	−0.37
Smad3 (SMAD family member 3)	Phospho-Ser^{425}	SMAD3	−0.37
c-Ab (ABL protooncogene 1, nonreceptor tyrosine kinase)	Phospho-Tyr^{412}	ABL1	−0.35
EPHA2/3/4 (EPH receptor A2/3/4)	Phospho-Tyr$^{588/596}$	EPHA2	−0.35
AKT1 (V-akt murine thymoma viral oncogene homolog 1)	Phospho-Thr^{308}	AKT1	−0.34
STAT5B (signal transducer and activator of transcription 5B)	Phospho-Ser^{731}	STAT5B	−0.33
FAK (protein tyrosine kinase 2)	Phospho-Tyr^{407}	PTK2	−0.32
IL-10R-α (interleukin-10 receptor, α)	Phospho-Tyr^{496}	IL10RA	−0.31
Rb (retinoblastoma 1)	Phospho-Ser^{811}	RB1	−0.31
CDK2 (cyclin-dependent kinase 2)	Phospho-Thr^{160}	CDK2	−0.30
DAB1 (Dab, reelin signal transducer, homolog 1)	Phospho-Tyr^{232}	DAB1	−0.30
Protein tyrosine kinase 2	Phospho-Tyr^{861}	PTK2	−1.23
Tyrosine hydroxylase	Phospho-Ser^{31}	TH	−0.30
WEE1 G2 checkpoint kinase	Phospho-Ser^{642}	WEE1	−0.30
Cyclin B1	Phospho-Ser^{126}	CCNB1	−0.29
PAK2 [p21 protein (Cdc42/Rac)-activated kinase 2]	Phospho-Ser^{192}	PAK2	−0.29
Tau (microtubule-associated protein-τ)	Phospho-Ser^{356}	MAPT	−0.28
Synaptotagmin I	Phospho-Ser^{309}	SYT1	−0.27
HER2 (Erb-b2 receptor tyrosine kinase 2)	Phospho-Thr^{686}	ERBB2	−0.27

ment score of 0.26 or higher, which is equivalent to a nonlog scale of 0.05.

Inquiry of these same datasets of candidate proteins using the GEO repository, limiting the search to studies performed in podocytes, revealed that all candidate proteins were identified as expressed in the transcriptome of the conditionally immortalized human podocyte cell line generated by Saleem et al. (43) according to expression profiling performed by Da Sacco et al. (9) using the Affymetrix Human Gene 1.0 ST microarray (NCBI GEO database accession GSE49439). In contrast, 17 of the proteins with differential phosphorylation patterns could not be located in the RNA sequencing expression database of mouse podocytes performed by Kann et al. (25) and available on the Renal Epithelial Transcriptome and Proteome Databases website (http://helixweb.nih.gov/ESBL/Database). Moreover, none of those proteins could be identified in the transcriptomic (Affymetrix Mouse Gene 1.0 ST microarray) and proteomic (SILAC) data on freshly isolated mouse podocytes recently published by Boerries et al. (7).

Pathway analysis of all the phosphoproteins represented in the array was carried out using the Kyoto Encyclopedia of Genes and Genomes (KEGG) function of the DAVID Bioinformatics Resources. This analysis revealed enrichment for 65 different signaling pathways, covering a variety of intracellular processes crucial for cell function. KEGG pathway analysis of candidate proteins revealed 11 pathways that were overrepresented among those with significant fold changes between FD and control podocytes (Table 7).

Table 6. *Gene set enrichment analysis*

GO Identifier	Term	Fold Enrichment	Bonferroni	Benjamini	FDR
GO:0051173	Positive regulation of nitrogen compound metabolic process	1.88	0.99	0.99	5.39
GO:0045597	Positive regulation of cell differentiation	2.28	1.00	1.00	11.02
GO:0051726	Regulation of cell cycle	1.92	1.00	0.98	11.69
GO:0040008	Regulation of growth	2.22	1.00	0.97	13.72
GO:004593	Positive regulation of nucleobase, nucleoside, nucleotide, and nucleic acid metabolic process	1.82	1.00	0.95	14.97

GO, Gene ontology; FDR, false discovery rate.

Table 7. *KEGG canonical pathways most represented in number of genes among the candidate proteins*

KEGG Pathway ID	Description	Count	*P* Value	Fold Enrichment	Bonferroni	Benjamini	FDR
hsa05200	Pathways in cancer	29	0.00013	1.80	0.0098	0.0098	0.13
hsa05220	Chronic myeloid leukemia	17	0.00024	2.41	0.0185	0.0093	0.25
hsa05212	Pancreatic cancer	15	0.00073	2.41	0.0550	0.0187	0.76
hsa05223	Nonsmall cell lung cancer	10	0.01998	2.20	0.7929	0.3254	19.23
hsa04010	MAPK signaling pathway	19	0.04409	1.49	0.9703	0.5051	37.93
hsa05210	Colorectal cancer	11	0.05134	1.82	0.9836	0.4960	42.73
hsa04660	T cell receptor signaling pathway	13	0.06122	1.64	0.9928	0.5053	48.74
hsa05215	Prostate cancer	13	0.06122	1.64	0.9928	0.5053	48.74
hsa05221	Acute myeloid leukemia	9	0.06919	1.91	0.9963	0.5030	53.16
hsa04370	VEGF signaling pathway	9	0.06919	1.91	0.9963	0.5030	53.16
hsa04012	ErbB signaling pathway	14	0.07944	1.54	0.9984	0.5120	58.34

DISCUSSION

We have generated disease-specific cell lines for in vitro modeling of Fabry podocytopathy. Changes in proteins involved in cell growth and differentiation and cell death were observed in CRISPR/Cas9 GLA-edited podocyte populations, which correlates well with reported differences in proliferation and/or cell death in FD podocytes compared with control podocytes.

The antibody microarray used in this study is enriched for 65 different signaling pathways that are relevant to human disease, several of which have been implicated in the pathogenesis of other glomerular diseases. Pathway analysis revealed that MAPK and VEGF pathways as well as nine other different signaling pathways are significantly enriched or overrepresented among our candidate proteins. Overall, our data are consistent with previous work by Lee et al. (29) FD mice, which suggested that both TGF-β and VEGF signaling contribute to FD nephropathy.

The MAPK pathway plays a critical role in kidney development (4, 10, 34, 54) and is activated in several animal models of glomerular disease, including puromycin-induced nephrosis, crescent glomerulonephritis, TGF-1 transgenic mice (55), diabetic nephropathy (26, 51), and Fabry nephropathy (29). The MAPK activation cascade consists of three sequentially activated protein kinases. p38 MAPK activated by hyperosmolarity, oxidative stress, and/or inflammatory cytokines leads to the phosphorylation of downstream targets and also to activation of nuclear transcription factors involved in the apoptosis response. We found changes in both the abundance and phosphorylation status of proteins within this pathway in CRISPR/Cas9 GLA-edited podocyte populations. Consistent with our data, Chuang et al. reported that advanced glycation end products trigger podocytes to undergo apoptosis via a p38-dependent pathway (18).

The TGF-β pathway also showed differences in protein abundance and phosphorylation in CRISPR/Cas9 GLA-edited podocytes compared with control cells. Perturbed TGF-β signaling has been implicated in the pathogenesis of renal fibrosis leading to focal segmental and global glomerulosclerosis seen in several chronic glomerular diseases, including FD (32, 48). Dysregulated TGF-β signaling is also thought to be a major contributor to podocyte epithelial mesenchymal transition (EMT). Jeon et al. (24) showed that Gb3 and Lyso-Gb3 strongly induced EMT in human proximal tubule HK2 cells, contributing to the development of renal fibrosis through the cell-specific induction of EMT in FD. Additionally, Sanchez-Niño and colleagues (44) showed that, in human immortalized podocytes, lyso-Gb3 increased the expression of TGF-β1, extracellular matrix proteins, and the macrophage inhibitory factor receptor CD74 in a dose- and time-dependent manner and that activation of vitamin D receptor prevents these effects. These data confirm that glycosphingolipid metabolites that accumulate in FD are biologically active and contribute to the development of podocytopathy and the progression of CKD.

A third pathway of interest highlighted by our phosphoarray analysis is the VEGF pathway. VEGF-A is an angiogenic growth factor produced in abundance by podocytes that plays an essential role in maintaining the integrity of the glomerular filtration barrier and functions as a survival factor for podocytes (21). Podocyte-specific VEGF-A excess or deficiency causes glomerular damage (53). Thus, it was expected that this pathway may be altered in our CRISPR/Cas9 model of FD and, indeed, we observed an enrichment of 1.9-fold compared with control. Abnormal VEGF signaling has also been observed in the diabetic nephropathy model, also regarded as a metabolic podocytopathy (23). Recently, a link has been established between the production of VEGF-A and the insulin signaling pathway in podocytes (19). Corroborating these findings, our microarray analysis found that CRISPR/Cas9 GLA-edited cells express significantly more insulin receptor than control cells (Table 2).

Phosphoproteomic studies are increasingly used to identify regulated protein interactions that contribute to glomerular function. A recent phosphoproteomic analysis of isolated mouse glomeruli identified 146 phosphorylation sites on proteins that are expressed at high levels in podocytes and confirmed a role for one such site in the formation of high-molecular-weight complexes of podocin (42). More recently, the same team (41) used a comparative phosphoproteomic analysis of mammalian glomeruli from several species to show that phosphorylation regulates the interaction between nephrin and CD2AP. These powerful approaches are likely to reveal new regulatory cascades that can be targeted in the clinical management of glomerular disease.

Our study presents some limitations to consider. Human immortalized podocytes maintained in culture fail to present some of the morphological and functional features observed in podocytes in vivo, such as interdigitating foot processes, as well as expression of slit diaphragm podocyte-specific proteins such as nephrin, which are crucial for podocyte function. Unfortunately, none of the podocyte-specific proteins was covered in our microarray. To the best of our knowledge, none

of the commercially available antibody microarrays allows for analysis of those podocyte-specific proteins. Another key point is that none of the components of the Coordinated Lysosomal Expression and Regulation gene network was represented in this study. Certainly some of these proteins would be expected to have different activation pattern in FD podocytes, which could not be detected using our approach. It is also possible that some differences in signaling revealed by the microarray analysis could potentially have derived from the CRISPR/Cas9 treatment itself. Finally, because phosphoproteomics methodology is in its early stages, interpretation of the results with respect to positive and negative effects on pathway activation is challenging.

In conclusion, antibody microarray analysis of our newly generated CRISPR/Cas9 GLA-edited podocyte populations supports previous findings in other models of FD and also suggests potential new avenues of exploration. Further study should enable the identification of candidate signaling pathways that may be modulated to interrupt the vicious cycle of the hyperfiltering nephron and could be translated to the clinic as an adjuvant therapy to enzyme replacement therapy to lessen the morbidity of chronic kidney disease in FD.

ACKNOWLEDGMENTS

M. L. Eshbach was supported by National Institute of Diabetes and Digestive and Kidney Diseases Grant T32-DK-061296.

DISCLOSURES

No conflicts of interest, financial or otherwise, are declared by the authors.

AUTHOR CONTRIBUTIONS

E.M.P., A.L., M.L.E., A.R., and A.R.S. performed experiments; E.M.P., A.L., and G.L. analyzed data; E.M.P., A.L., S.M., and O.A.W. interpreted results of experiments; E.M.P. prepared figures; E.M.P., S.M., and O.A.W. edited and revised manuscript; E.M.P., S.M., and O.A.W. approved final version of manuscript; A.L., S.M., and O.A.W. conception and design of research.

REFERENCES

1. **Alroy J, Sabnis S, Kopp JB.** Renal pathology in Fabry disease. *J Am Soc Nephrol* 13: S134–S138, 2002.
2. **Anderson W.** A case of "angeio-keratoma." *Br J Dermatol* 10: 113–117, 1898.
3. **Ashburner M, Ball CA, Blake JA, Botstein D, Butler H, Cherry JM, Davis AP, Dolinski K, Dwight SS, Eppig JT.** Gene Ontology: tool for the unification of biology. *Nat Genet* 25: 25–29, 2000.
4. **Balbi A, Francescato H, Marin E, Costa R, Coimbra T.** Roles of mitogen-activated protein kinases and angiotensin II in renal development. *Br J Medi Biol Res* 42: 38–43, 2009.
5. **Barrett T, Wilhite SE, Ledoux P, Evangelista C, Kim IF, Tomashevsky M, Marshall KA, Phillippy KH, Sherman PM, Holko M.** NCBI GEO: archive for functional genomics data sets-update. *Nucleic Acids Res* 41: D991–D995, 2013.
6. **Becherucci F, Romagnani P.** When foots come first: early signs of podocyte injury in Fabry nephropathy without proteinuria. *Nephron* 129: 3–5, 2015.
7. **Boerries M, Grahammer F, Eiselein S, Buck M, Meyer C, Goedel M, Bechtel W, Zschiedrich S, Pfeifer D, Laloë D.** Molecular fingerprinting of the podocyte reveals novel gene and protein regulatory networks. *Kidney Int* 83: 1052–1064, 2013.
8. **Brady RO, Gal AE, Bradley RM, Martensson E, Warshaw AL, Laster L.** Enzymatic defect in Fabry's disease: ceramidetrihexosidase deficiency. *N Engl J Med* 276: 1163–1167, 1967.
9. **Da Sacco S, Lemley KV, Sedrakyan S, Zanusso I, Petrosyan A, Peti-Peterdi J, Burford J, De Filippo RE, Perin L.** A novel source of cultured podocytes. *PloS one* 8: e81812, 2013.
10. **de Haij S, Daha MR, Van Kooten C.** Mechanism of steroid action in renal epithelial cells. *Kidney Int* 65: 1577–1588, 2004.
11. **Deegens JK, Dijkman HB, Borm GF, Steenbergen EJ, van den Berg JG, Weening JJ, Wetzels JF.** Podocyte foot process effacement as a diagnostic tool in focal segmental glomerulosclerosis. *Kidney Int* 74: 1568–1576, 2008.
12. **Delarue F, Virone A, Hagege J, Lacave R, Peraldi MN, Adida C, Rondeau E, Feunteun J, Sraer JD.** Stable cell line of T-SV40 immortalized human glomerular visceral epithelial cells. *Kidney Int* 40: 906–912, 1973.
13. **Drenckhahn D, Franke R.** Ultrastructural organization of contractile and cytoskeletal proteins in glomerular podocytes of chicken, rat, and man. *Lab Invest* 59: 673–682, 1988.
14. **Edgar R, Domrachev M, Lash AE.** Gene Expression Omnibus: NCBI gene expression and hybridization array data repository. *Nucleic Acids Res* 30: 207–210, 2002.
15. **Fabry J.** Ein beitrag zur kenntniss der purpura haemorrhagica nodularis (purpura papulosa haemorrhagica hebrae). *Arch Dermatol Res* 43: 187–200, 1898.
16. **Farquhar MG.** The glomerular basement membrane: not gone, just forgotten. *J Clin Invest* 116: 2090–2093, 2006.
17. **Fukasawa H, Bornheimer S, Kudlicka K, Farquhar MG.** Slit diaphragms contain tight junction proteins. *J Am Soc Nephrol* 20: 1491–1503, 2009.
18. **Goh KC, Williams BR.** The protein kinase PKR is required for p38 MAPK activation and the innate immune response to bacterial endotoxin. *EMBO J* 19: 4292–4297, 2000.
19. **Hale LJ, Hurcombe J, Lay A, Santamaría B, Valverde AM, Saleem MA, Mathieson PW, Welsh GI, Coward R.** Insulin directly stimulates VEGF-A production in the glomerular podocyte. *Am J Physiol Renal Physiol* 305: F182–F188, 2013.
20. **Hornbeck PV, Kornhauser JM, Tkachev S, Zhang B, Skrzypek E, Murray B, Latham V, Sullivan M.** PhosphoSitePlus: a comprehensive resource for investigating the structure and function of experimentally determined post-translational modifications in man and mouse. *Nucleic Acids Res* gkr1122, 2011.
21. **Hovind P, Tarnow L, Oestergaard PB, Parving HH.** Elevated vascular endothelial growth factor in type 1 diabetic patients with diabetic nephropathy. *Kidney Int* 57: S56–S61, 2000.
22. **Huang DW, Sherman BT, Lempicki RA.** Systematic and integrative analysis of large gene lists using DAVID bioinformatics resources. *Nat Protocols* 4: 44–57, 2009.
23. **Jefferson J, Shankland S, Pichler R.** Proteinuria in diabetic kidney disease: a mechanistic viewpoint. *Kidney Int* 74: 22–36, 2008.
24. **Jeon YJ, Jung N, Park JW, Park HY, Jung SC.** Epithelial-mesenchymal transition in kidney tubular epithelial cells induced by globotriaosylsphingosine and globotriaosylceramide. *PloS one* 10: e0136442, 2015.
25. **Kann M, Ettou S, Jung YL, Lenz MO, Taglienti ME, Park PJ, Schermer B, Benzing T, Kreidberg JA.** Genome-wide analysis of wilms' tumor 1-controlled gene expression in podocytes reveals key regulatory mechanisms. *J Am Soc Nephrol* ASN. 2014090940, 2015.
26. **Kikkawa R, Koya D, Haneda M.** Progression of diabetic nephropathy. *Am J Kidney Dis* 41: S19–S21, 2003.
27. **Kint J.** Fabry's disease: alpha-galactosidase deficiency. *Science* 167: 1268–1269, 1970.
28. **Korbie DJ, Mattick JS.** Touchdown PCR for increased specificity and sensitivity in PCR amplification. *Nat Protocols* 3: 1452–1456, 2008.
29. **Lee MH, Choi EN, Jeon YJ, Jung SC.** Possible role of transforming growth factor-β1 and vascular endothelial growth factor in Fabry disease nephropathy. *Int J Mol Med* 30: 1275–1280, 2012.
30. **Mayes JS, Cray EL, Dell VA, Scheerer J, Sifers R.** Endocytosis of lysosomal alpha-galactosidase A by cultured fibroblasts from patients with Fabry disease. *Am J Human Genet* 34: 602, 1982.
31. **Mayes JS, Scheerer JB, Sifers RN, Donaldson ML.** Differential assay for lysosomal alpha-galactosidases in human tissues and its application to Fabry's disease. *Clin Chim Acta* 112: 247–251, 1981.
32. **Meng XM, Huang XR, Chung AC, Qin W, Shao X, Igarashi P, Ju W, Bottinger EP, Lan HY.** Smad2 protects against TGF-β/Smad3-mediated renal fibrosis. *J Am Soc Nephrol* 21: 1477–1487, 2010.
33. **Mundel P, Shankland SJ.** Podocyte biology and response to injury. *J Am Soc Nephrol* 13: 3005–3015, 2002.
34. **Omori S, Hida M, Ishikura K, Kuramochi S, Awazu M.** Expression of mitogen-activated protein kinase family in rat renal development. *Kidney Int* 58: 27–37, 2000.

35. **Opitz JM, Stiles FC, Wise D, Race R, Sanger R, Von Gemmingen GR, Kierland RR, Cross EG, De Groot W.** The genetics of angiokeratoma corporis diffusum (Fabry's disease) and its linkage relations with the Xg locus. *Am J Human Genet* 17: 325, 1965.
36. **Oqvist B, Brenner BM, Oliveira JP, Ortiz A, Schaefer R, Svarstad E, Wanner C, Zhang K, Warnock DG.** Nephropathy in Fabry disease: the importance of early diagnosis and testing in high-risk populations. *Nephrol Dial Transplan* 24: 1736–1743, 2009.
37. **Pavenstädt H, Kriz W, Kretzler M.** Cell biology of the glomerular podocyte. *Physiol Rev* 83: 253–307, 2003.
38. **Pereira EM, Labilloy A, da Silva AS, Neto J, do Monte SJ.** Podocyturia in Fabry disease: a tool for monitoring renal disorders. *Mol Genet Metab* 111: S85–S86, 2014.
39. **Ponchiardi C, Fall B, Scott R, Uhrich S, Mauer M, Whitley C, Pippin J, Shankland S, Jefferson J, Najafian B.** Podocyturia correlates with proteinuria in patients with Fabry disease (FD) and is a potential biomarker of Fabry nephropathy. *Mol Genet Metab* 108: S76–S77, 2013.
40. **Ramakrishna S, Cho SW, Kim S, Song M, Gopalappa R, Kim JS, Kim H.** Surrogate reporter-based enrichment of cells containing RNA-guided Cas9 nuclease-induced mutations. *Nat Commun* 5, 2014.
41. **Rinschen MM, Benzing T, Limbutara K, Pisitkun T.** Proteomic analysis of the kidney filtration barrier-Problems and perspectives. *Proteomics Clin App* 9: 1053–1068, 2015.
42. **Rinschen MM, Schermer B, Benzing T.** Vasopressin-2 receptor signaling and autosomal dominant polycystic kidney disease: from bench to bedside and back again. *J Am Soc Nephrol* 25: 1140–1147, 2014.
43. **Saleem MA, O'Hare MJ, Reiser J, Coward RJ, Inward CD, Farren T, Xing CY, Ni L, Mathieson PW, Mundel P.** A conditionally immortalized human podocyte cell line demonstrating nephrin and podocin expression. *J Am Soc Nephrol* 13: 630–638, 2002.
44. **Sanchez-Niño MD, Sanz AB, Carrasco S, Saleem MA, Mathieson PW, Valdivielso JM, Ruiz-Ortega M, Egido J, Ortiz A.** Globotriaosylsphingosine actions on human glomerular podocytes: implications for Fabry nephropathy. *Nephrol Dial Transplan*: gfq306, 2010.
45. **Schiffmann R, Waldek S, Benigni A, Auray-Blais C.** Biomarkers of Fabry disease nephropathy. *Clin J Am Soc Nephrol* 5: 360–364, 2010.
46. **Sessa A, Meroni M, Battini G, Maglio A, Brambilla P, Bertella M, Nebuloni M, Pallotti F, Giordano F, Bertagnolio B.** Renal pathological changes in Fabry disease. *J Inher Metab Dis* 24: 66–70, 2001.
47. **Shibata A, Jeggo P.** DNA double-strand break repair in a cellular context. *Clin Oncol* 26: 243–249, 2014.
48. **Svarstad E, Bostad L, Kaarbøe Ø, Houge G, Tøndel C, Lyngdal P, Iversen B.** Focal and segmental glomerular sclerosis (FSGS) in a man and a woman with Fabry's disease. *Clin Nephrol* 63: 394–401, 2005.
49. **Team RC.** *R: A Language and Environment for Statistical Computing*. Vienna, Austria: R Foundation for Statistical Computing, 2014.
50. **Tøndel C, Bostad L, Hirth A, Svarstad E.** Renal biopsy findings in children and adolescents with Fabry disease and minimal albuminuria. *Am J Kidney Dis* 51: 767–776, 2008.
51. **Toyoda M, Suzuki D, Honma M, Uehara G, Sakai T, Umezono T, Sakai H.** High expression of PKC-MAPK pathway mRNAs correlates with glomerular lesions in human diabetic nephropathy. *Kidney Int* 66: 1107–1114, 2004.
52. **Valbuena C, Leitão D, Carneiro F, Oliveira JP.** Immunohistochemical diagnosis of Fabry nephropathy and localisation of globotriaosylceramide deposits in paraffin-embedded kidney tissue sections. *Virchows Arch* 460: 211–221, 2012.
53. **Veron D, Reidy KJ, Bertuccio C, Teichman J, Villegas G, Jimenez J, Shen W, Kopp JB, Thomas DB, Tufro A.** Overexpression of VEGF-A in podocytes of adult mice causes glomerular disease. *Kidney Int* 77: 989–999, 2010.
54. **Yim HE, Yoo KH, Bae IS, Jang GY, Hong YS, Lee JW.** Aldosterone regulates cellular turnover and mitogen–activated protein kinase family expression in the neonatal rat kidney. *J Cell Physiol* 219: 724–733, 2009.
55. **Zeisberg M, Kalluri R.** The role of epithelial-to-mesenchymal transition in renal fibrosis. *J Mol Med* 82: 175–181, 2004.